(IJIEST) 2025, Vol. No. 11, Issue 1, Jan-Dec **e-ISSN: 2454-9584; p-ISSN: 2454-8111**

Smart Homes Chip Free Light Switch

Basim Abdul Kareem Farhan, Nawar Banwan Hassan, Wisam Ali Hasan
Department of Computer Techniques Engineering
Imam Al-Kadhum University College (IKC)
Baghdad, Iraq

DOI: 10.37648/ijps.v11i01.001

[1]*Date of Receiving: 27 October 2024; Date of Acceptance: 03 December 2024; Date of Publication: 02 January 2025*

ABSTRACT

Recent advancements in wireless sensor technology have surpassed the capabilities of conventional light switches, leading to the development of chipless RFID light switches (CLS). This novel CLS is designed to be passive, operate without batteries, and maintain portability while preserving the familiar tactile experience of physical buttons for controlling devices such as light bulbs.

The CLS architecture incorporates toggle switches connected to radiofrequency spiral resonators. These resonators passively communicate the switch status through activation or deactivation by manipulating the switches. To construct the CLS tag, an FR4 substrate with a thickness of 1 mm was utilized. This substrate comprised two identification resonators and two measurement resonators (MRs) for transmitting the status information.

Experimental findings demonstrated resonant frequencies of 1115 and 1220 MHz for the identification resonators, whereas the MRs exhibited 848 and 971 MHz frequencies. Successful toggling of the switches between the ON and OFF states resulted in the corresponding activation or deactivation of MRs.

Keywords: *light switches; CLS; smart homes; wireless sensors; chipless*

INTRODUCTION

In 1884, a quick-break mechanism, the earliest form of the light switch, was developed. The light switch design remained largely unaltered until recently, consisting of an electrical switch with an internal quick-break mechanism and wires connecting the switch to electrical devices such as light bulbs or air conditioners[1]. Although this conventional approach is user-oriented, it offers limited functionality and utility. However, the traditional light switches have several limitations.

1. They are positioned in fixed locations within a room, which may not be optimal or adaptable to various requirements, often necessitating users to approach the switch physically.

2. They require impractical infrastructure, such as extensive wiring installed through walls, to connect switches with light fixtures and power sources.

3. Once installed, it is challenging to repurify the alternative applications.

[1] *How to cite the article:*
Farhan B.A.K., Hassan N.B., Hasan W.A., (2025) Smart Homes Chip Free Light Switch; *International Journal of Inventions in Engineering and Science Technology*, Vol 11 Issue 1, 1-9

The limitations of traditional light switches include various switch types utilized in residential, vehicular, healthcare, retail, exhibition, and other environments. Contemporary Internet of Things (IoT) solutions incorporate voice-activated assistants, battery-powered remote controls, motion-detecting switches, and smartphone applications [1][2]. While these IoT switches can augment conventional switches, they cannot fully supply them because their reliable operation is contingent on specific conditions. For example, voice assistants exhibit reduced efficacy in high-noise environments [2], smartphones require prior connectivity (rendering them inoperable in public spaces), batteries are inevitably depleted [3], and motion sensors may be inadvertently triggered by unintended movements.

The modernization of light switches has become increasingly viable due to advancements in wireless sensor technology [4][5]. Wireless sensors offer the distinct advantage of eliminating the requirement for wires or batteries, thereby enabling their relocation and attachment to diverse surfaces. This development has transformed the conceptualization of light switches to resemble passive remote controls for operating electrical devices (such as light bulbs and televisions).

A wireless sensor can be constructed by incorporating a radio frequency (RF) identification integrated circuit (chipped RFID) into a wireless device [6][7]. This chipped RFID utilizes the RF energy from its environment to power the electronic components of the device. These components subsequently collect sensor data, encode it, and wirelessly transmit the information to a central hub (CH) [6]. Chipped RFIDs are recognized for their comparatively high data transmission rates and capacity to operate across substantial distances [8].

CL-RFID, or chipless RFID, presents an alternative approach to wireless sensing and object identification by examining spectral signatures [9][10]. CL-RFIDs are fabricated using planar encoders, which are RF resonators featuring specific patterns that contain ID code. In contrast to chipped RFIDs, CL-RFIDs do not incorporate integrated circuits, potentially resulting in significantly reduced production costs [11]. Moreover, CL-RFIDs can be applied to conventional fabrics using conductive ink, rendering them a viable option for wearable electronic applications [11].

A typical CL-RFID system comprises two primary components: a CL-RFID reader (also referred to as an interrogator) and CL-RFID tag (the item being monitored). The reader transmits a wide-spectrum interrogation signal, and subsequently decodes the signal reflected by the tag. The tag encodes data into the reflected signal utilizing either time-delay units in the time domain or RF resonators in the frequency domain [12]. Each RF resonator was designed to resonate at a specific frequency, and each time-delay unit was constructed with a particular delay. By analyzing this information from the reflected signal, it becomes feasible to track, sense, and identify the proximate CL-RFID tags.

The spectral signature of a CL-RFID tag is determined by the physical properties of its time delay elements and RF resonators. Typically, the CL-RFID tag employed for wireless sensing incorporates several elements. Some of these elements possess fixed electrical properties and are utilized for tag identification, whereas others exhibit variable characteristics (such as adjustable frequency or delays) and are employed to convey measurement data. Variable characteristics are achieved by rendering one of the elements sensitive to environmental factors, such as temperature or humidity. Consequently, when the ambient conditions change, the value of one of the resonant frequencies (or delay elements) also changes [13].

Various sensing applications have used CL-RFIDs. Amin et al. [9] developed a printable, cost-effective CL-RFID humidity sensor, wherein humidity alters the tag's resonant frequency. Fang et al. [10] designed a CL-RFID sensor tag for package identification and humidity monitoring using two inductor-capacitor resonators, one with a fixed resonant frequency and another with a variable one. Marindra et al. [14] engineered a CL-RFID system for metal crack detection using tip-loaded dipole resonators. Brinker et al. [15] developed a CL-RFID pressure sensor in which pressure on the tag modifies the resonant frequency.[16]

This paper introduces a novel chipless switch (CLS) that is wireless, battery-free, portable, and economical. The CLS can be applied to various surfaces, enabling wireless control of light bulbs and other electrical devices, such as televisions. Based on CL-RFID technology, the CLS tag aims to transform the conventional light switch concept by utilizing switches to control the spectral signature of the tag. While maintaining the practicality of physical interactions, CLS incorporates simplicity, accessibility, and convenience. CLS can be affixed to items such as book covers or clothing, enabling users to manipulate their surroundings with minimal physical effort.

PROPOSED MODEL DESIGN

CLS system overview

The proposed CLS system, illustrated in Figure 1, comprises a central hub (C.H.) and a battery-free remote unit (CLS tag). The C.H. incorporates a trans receiving antenna, a chipless RFID reader, and a controller linked to various devices such as light bulbs and televisions. The tag features receive and transmit antennas connected by a transmission line, along with electromagnetic resonators (ID resonators [IDRs] and measurement resonators [M.R.s]) coupled to the transmission line and switches (physical buttons) attached to the MRs. IDRs serve tag identification, while M.R.s communicate the switch status. This configuration enables the C.H. to wirelessly power and retrieve data from multiple CLS tags by emitting a continuous wideband interrogation signal. The C.H. subsequently interprets the received data to manage connected devices.

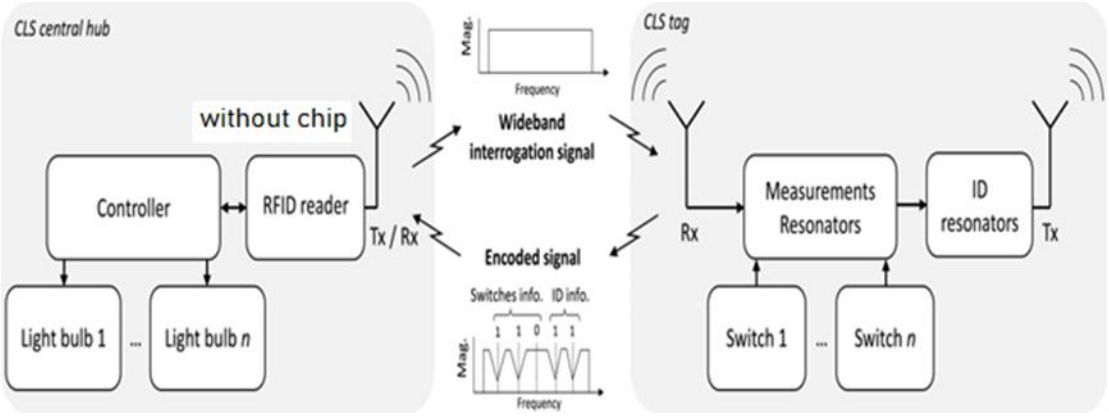

Figure 1. In the CLS system, the C.H. transmits a wideband signal that powers the tag wirelessly, reads the reflected encoded signals, and regulates the attached light bulbs accordingly. The tag captures the wideband signal, passively incorporates the switch status and ID information, and returns the encoded signal.

The process of wireless powering and signal reading by the C.H. involves broadcasting a wideband signal, which is detected by the receiving antenna of the tag and transmitted through the transmission line. The resonators coupled to the transmission line create nulls at specific frequencies in the received signal corresponding to their resonant frequencies. This encoding process results in nulls at the resonant frequencies of the active resonators, whereas inactive resonators do not affect the wideband signal. Notably, switches linked to the M.R.s can activate or deactivate them. An OFF button activates the corresponding M.R., whereas an ON switch deactivates it. Consequently, the resulting wideband signal encodes information from both active and inactive resonators, reflecting the status of the switches. The transmitting antenna of the tag sends this encoded signal back to the C.H., which receives, processes, and utilizes it to control the various devices.

CLS tag

A CLS tag comprising four spiral resonators (consisting of two IDRs and two M.R.s) connected to a microstrip line and two switches is depicted in Figure 2a. The number of resonant elements can be modified by incorporating or removing the resonators, as required. In this study, the antennas responsible for reception and transmission were designated as Rx/Tx ports. The spiral resonators were positioned close to the microstrip line to facilitate coupling. This proximity enables electromagnetic interactions between the transmission line and resonators. Consequently, the resonant frequencies of the spiral resonators are coupled to the transmission line, resulting in nulls in the encoded signal.

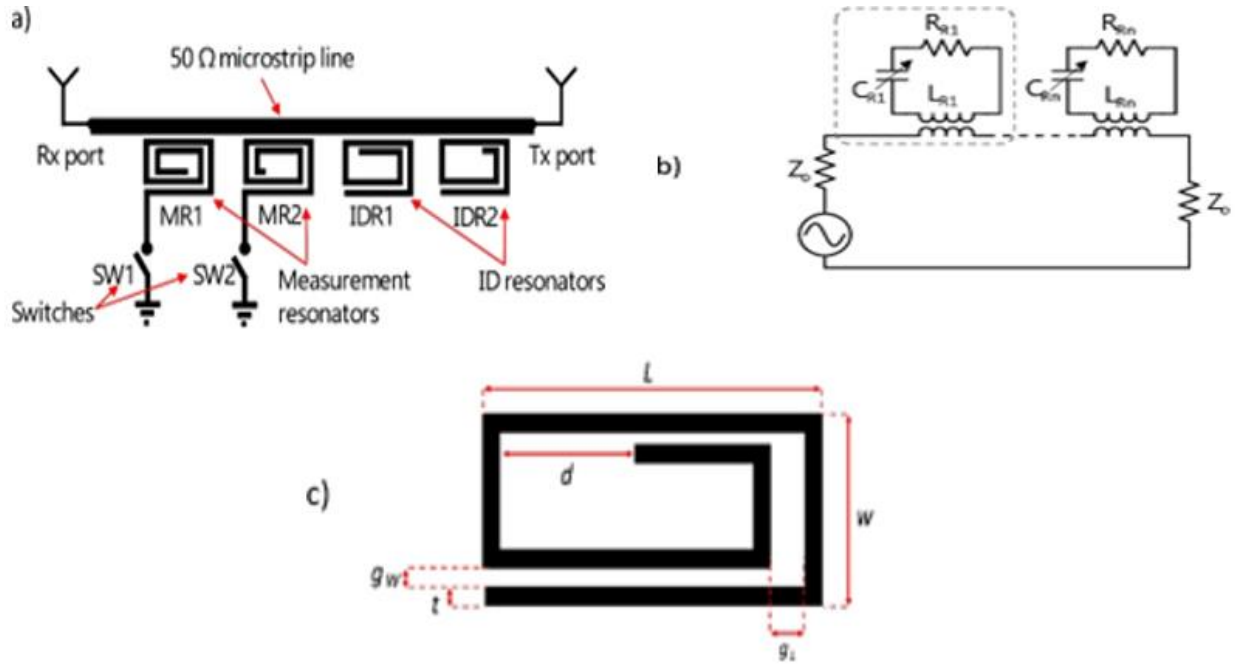

Figure 2. (a) The proposed CLS tag comprises four spiral resonators coupled to a 50-Ω transmission line. Two of these resonators function as measurement resonators (MR1, 2), while the other two serve as I.D. resonators (IDR1, 2). Furthermore, the design incorporated two switches that connected the termini of the sensing resonators to the ground plane. (b) CLS tag's equivalent circuit is represented by multiple RLC tanks. (c) The spiral resonators exhibited specific design parameters.

Table (1) Resonator dimensions

Pole	**MR1**	**MR2**	**IDR1**	**IDR2**
Turns	2.250	2.250	1.750	1.750
L	15.90	15.90	15.90	15.90
W	6.0	6.0	6.0	6.0
T	0.40	0.40	0.40	0.40
g_L	0.80	0.80	0.80	0.80
g_W	1.0	1.0	1.0	1.0
D	0.70	8.0	1.40	6.90

(Note: All dimensions are in millimeters.)

An (E.M.) simulation of a CLS tag, comprising two M.R.s (MR1, 2) and two IDRs (IDR1, 2), is depicted in Figure 3. This simulation, conducted utilizing the Keysight Advanced Design System ADS, operates at a frequency of 1.02 GHz, which corresponds to MR1's resonant frequency. The E.M. simulation demonstrates that when MR1's switch is in the OFF position (open-circuit, disconnected from the ground plane), MR1 exhibits resonance that couples with the microstrip line. Conversely, when MR1's switch is ON (short-circuited, connected to the ground plane), MR1 ceases to resonate and does not affect the performance of the microstrip line.

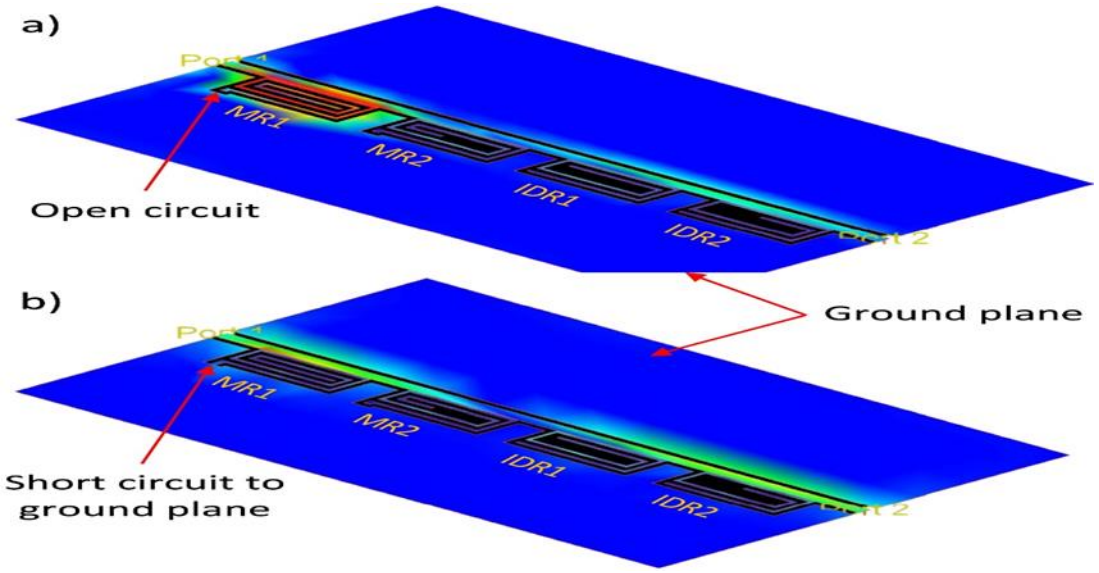

Figure 3. Electromagnetic simulation depicting the current distribution in a CLS tag. (a) When the switch associated with the measurement resonators [MR1] is in the OFF state (i.e., MR1 functions as an open circuit relative to the ground plane), MR1 demonstrates resonance at its characteristic frequency fMR1. (b) When the switch associated with MR1 is in the ON state (i.e., MR1 operates as a short-circuit to the ground plane), MR1 does not exhibit resonance at fMR1.

The simulation outcomes of the encoded signal (insertion loss S21) for the CLS tag, depicted in Figure 2, are illustrated in Figure 4. When all switches are in the OFF position, each resonator is operational, resulting in S21 exhibiting four nulls at the resonant frequencies of the resonators (fMR1, 2, and fIDR1, 2). It is noteworthy that MR1's largest dimensions generated the lowest resonant frequency at 1.02 GHz. Conversely, IDR2, which was the smallest, produced the highest resonant frequency of 1.31 GHz. The resonant frequencies of MR2 and IDR1 are 1.1 and 1.2 GHz, respectively. Activation of either SW1 or SW2 deactivates the corresponding resonator by grounding it. In the dashed line in Figure 4, only SW1 is activated, resulting in the elimination of the associated null at 1.02 GHz.

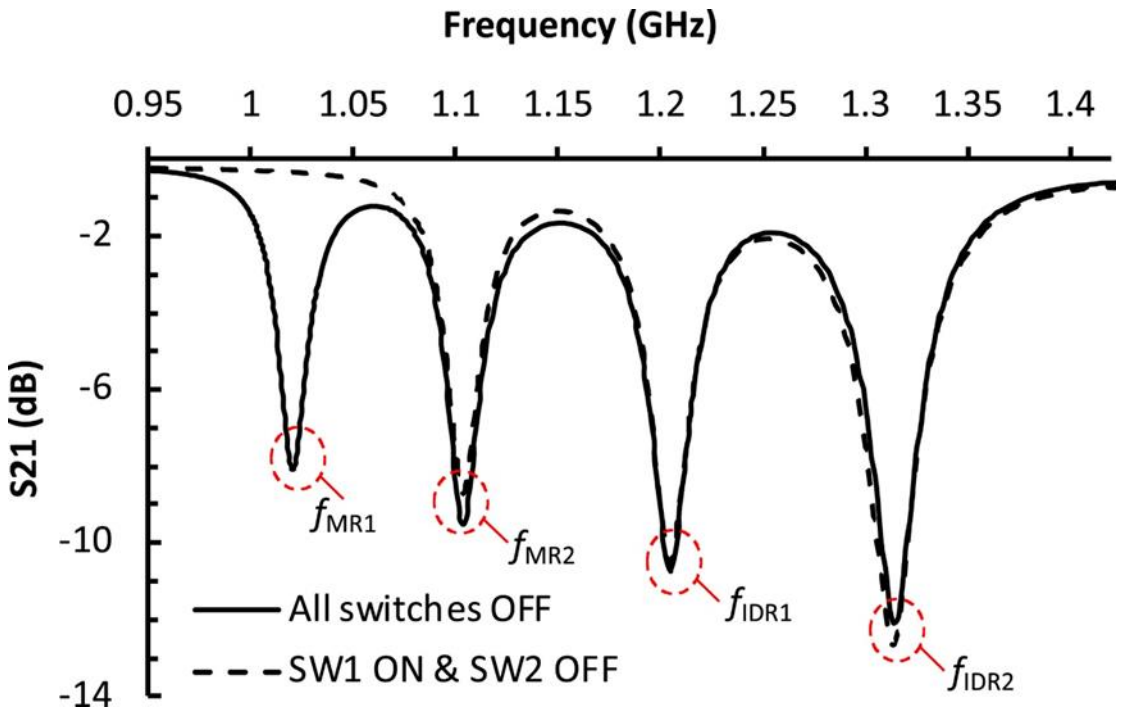

Figure 4. shows the simulated insertion loss results for the switches in the OFF and ON positions. The solid line depicts a scenario in which all buttons are OFF, demonstrating that the encoded signal exhibits nulls at frequencies fMR1, fMR2, fIDR1, and fIDR2. These frequencies correspond to the measurement resonators MR1, MR2, IDR1, and IDR2, respectively.

MEASUREMENTS RESULTS

The CLS tag was fabricated on a 1-mm, 2-layer FR4 substrate with a dielectric constant of 4.6. Figure 5 shows the fabricated tags. The dimensions of the tags were 94 mm × 60 mm. Commercially available single-pole-single-through (SPDT) toggle switches were used. For measurement purposes, a calibrated R.F. analyzer (FieldFox N9912A) was directly connected to the Tx and Rx ports of the CLS tag.

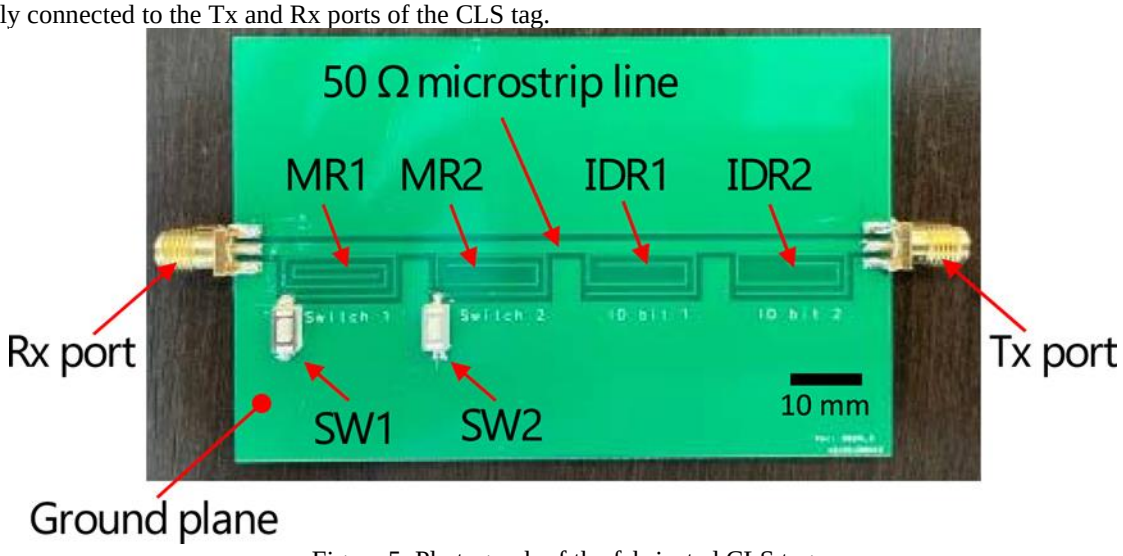

Figure 5. Photograph of the fabricated CLS tag

(IJIEST) 2025, Vol. No. 11, Issue 1, Jan-Dec **e-ISSN: 2454-9584; p-ISSN: 2454-8111**

The measurement results of the insertion loss for the ON and OFF switch states are shown in Figure 6. When both switches (SW1 and SW2) are in the OFF state, all resonators (MR1, MR2, IDR1, and IDR2) are operational, resulting in four nulls in the S21 parameter at their respective resonant frequencies (fMR1, fMR2, fIDR1, and fIDR2), as illustrated in Figure 6a. Measurements indicated that the frequencies of MR1, MR2, IDR1, and IDR2 were 848, 971, 1115, and 1220 MHz, respectively. The activation of the switches is grounded and deactivated MR1, MR2, and MR3, thereby eliminating their corresponding resonant frequencies (fMR1 and fMR2). The resonant frequencies (fIDR1 and fIDR2) associated with IDR1 remained constant and unaffected by SW1 and SW2. Figure 6b presents the measurement results when SW1 and SW2 were in the ON state, demonstrating the cancellation of the corresponding null at 848 and 971 MHz, respectively. Notably, the measured fMR1 and fMR2 values exhibited a shift of up to 172 MHz compared to the simulation results. This frequency shift was attributed to the additional switch length, which was not considered in the simulation. Furthermore, the measured insertion losses at fMR1 and fMR2 were up to 3.7 dB higher than the simulated values, owing to the additional losses introduced by the switches.

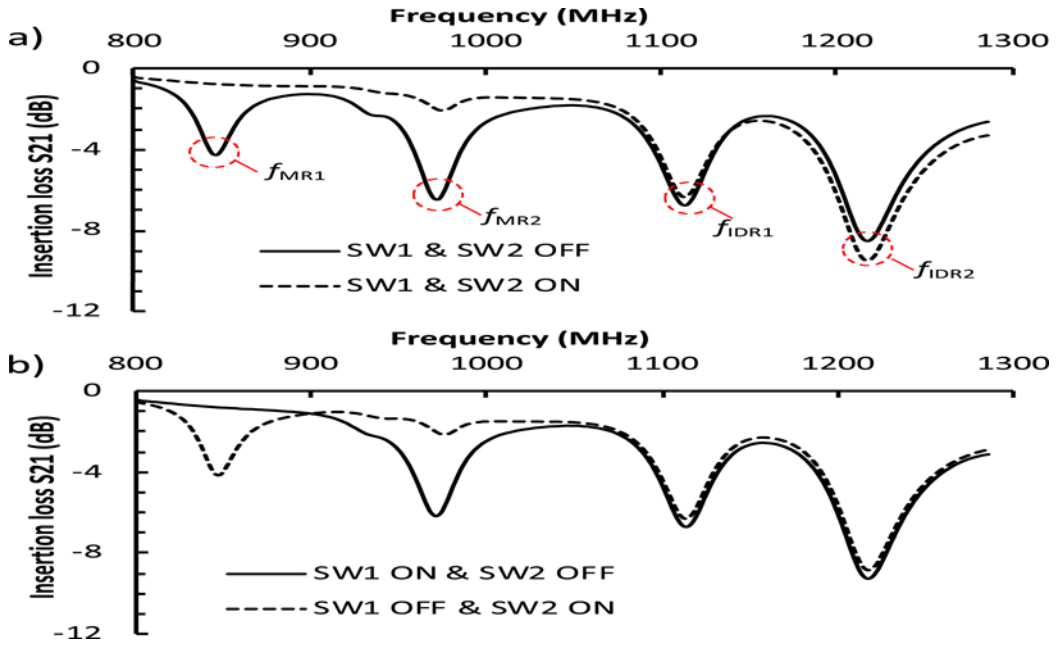

Figure 6. shows the CLS-tag measurement results. Panel (a) depicts the outcomes when all switches are either deactivated or activated, whereas panel (b) illustrates the scenario in which one controller is deactivated. The activation of the switch eliminates the corresponding resonant frequency. The resonant frequencies at fIDR1 and 2 remain unaffected by the switch status and were consistently present for tag identification purposes.

SIMULATION AND DISCUSSION

The research indicates that The proposed filtering antenna design, illustrated in Figure 5, was developed and optimized using Computer Simulation Technology (CST) software. The optimized coupling spacing distance (S) for the filtering antenna design was demonstrated through the simulated S11 - Parameter and gain. The performance of the filtering antenna design improved as the coupling space (S) increased. The design parameters of the filtering antenna demonstrate superior specifications compared to a conventional patch antenna operating under similar conditions. Table 1 presents a comprehensive comparison of the design parameters of the innovative filtering antenna design and standard patch antenna design.

CONCLUSION

The CLS light switch is an innovative device that integrates wireless functionality with the familiarity of physical buttons without requiring batteries and at a cost-effective price point. These features were achieved by connecting readily available single-pole single-throw switches between spiral resonators and a grounding plane. The activation

or deactivation of the switch enables or disables the resonator, respectively, allowing the CLS label to passively communicate the status of the buttons to a CH.

REFERENCES

1. A. Lucero, J. Mason, A. Wiethoff, B. Meerbeek, H. Pihlajaniemi, and D. Aliakseyeu, "Rethinking our interactions with light," *Interactions*, vol. 23, no. 6, pp. 54–59, 2016.
2. A. A.-I. S. Letters and undefined 2023, "Tactile Light Switch Using Chipless RFID," *ieeexplore.ieee.org*, Accessed: Dec. 04, 2023. [Online]. Available: https://sci-hub.ren/https://ieeexplore.ieee.org/abstract/document/10209163/
3. A. Almansouri, … M. O.-I. T. on, and undefined 2018, "A CMOS RF-to-DC power converter with 86% efficiency and− 19.2-dBm sensitivity," *ieeexplore.ieee.orgAS Almansouri, MH Ouda, KN SalamaIEEE Transactions on Microwave Theory and Techniques, 2018•ieeexplore.ieee.org*, Accessed: Dec. 04, 2023. [Online]. Available: https://sci-hub.ren/https://ieeexplore.ieee.org/abstract/document/8252773/
4. S. Olenik, H. Lee, F. G.-N. R. Materials, and undefined 2021, "The future of near-field communication-based wireless sensing," *nature.comS Olenik, HS Lee, F GüderNature Reviews Materials, 2021•nature.com*, Accessed: Dec. 06, 2023. [Online]. Available: https://sci-hub.ren/https://www.nature.com/articles/s41578-021-00299-8
5. H. Landaluce, L. Arjona, A. Perallos, F. Falcone, I. Angulo, and F. Muralter, "A review of IoT sensing applications and challenges using RFID and wireless sensor networks," *mdpi.comH Landaluce, L Arjona, A Perallos, F Falcone, I Angulo, F Muralter Sensors, 2020•mdpi.com*, doi: 10.3390/s20092495.
6. M. Ouda, M. Arsalan, … L. M.-I. T., and undefined 2013, "5.2-GHz RF power harvester in 0.18-/spl mu/m CMOS for implantable intraocular pressure monitoring," *ieeexplore.ieee.orgMH Ouda, M Arsalan, L Marnat, A Shamim, KN SalamaIEEE Transactions on Microwave Theory and Techniques, 2013•ieeexplore.ieee.org*, Accessed: Dec. 06, 2023. [Online]. Available: https://sci-hub.ren/https://ieeexplore.ieee.org/abstract/document/6495731/
7. A. S. Almansouri, J. Kosel, and K. N. Salama, "A dual-mode nested rectifier for ambient wireless powering in CMOS technology," *IEEE Transactions on Microwave Theory and Techniques*, vol. 68, no. 5, pp. 1754–1762, 2020.
8. C. Herrojo, F. Paredes, J. Mata-Contreras, F. M.- Sensors, and undefined 2019, "Chipless-RFID: A review and recent developments," *mdpi.comC Herrojo, F Paredes, J Mata-Contreras, F Martín Sensors, 2019•mdpi.com*, Accessed: Dec. 06, 2023. [Online]. Available: https://sci-hub.ren/https://www.mdpi.com/1424-8220/19/15/3385
9. B. Winther-Jensen, E. M. Amin, M. Shakil Bhuiyan, N. C. Karmakar, and B. Winther-Jensen, "Development of a low cost printable chipless RFID humidity sensor," *ieeexplore.ieee.orgEM Amin, MS Bhuiyan, NC Karmakar, B Winther-Jensen IEEE sensors Journal, 2013•ieeexplore.ieee.org*, vol. 14, no. 1, 2014, doi: 10.1109/JSEN.2013.2278560.
10. Y. Feng, L. Xie, Q. Chen, L. Z.-I. S. Journal, and undefined 2014, "Low-cost printed chipless RFID humidity sensor tag for intelligent packaging," *ieeexplore.ieee.orgY Feng, L Xie, Q Chen, LR ZhengIEEE Sensors Journal, 2014•ieeexplore.ieee.org*, Accessed: Dec. 06, 2023. [Online]. Available: https://sci-hub.ren/https://ieeexplore.ieee.org/abstract/document/6995967/
11. S. B.-I. S. Journal and undefined 2021, "Chipless RFID sensors for wearable applications: A review," *ieeexplore.ieee.orgSK BeheraIEEE Sensors Journal, 2021•ieeexplore.ieee.org*, Accessed: Dec. 06, 2023. [Online]. Available: https://sci-hub.ren/https://ieeexplore.ieee.org/abstract/document/9606752/
12. S. Preradovic and N. C. Karmakar, *Multiresonator-based chipless RFID: barcode of the future*. Springer Science & Business Media, 2012.
13. S. Dey, J. K. Saha, and N. C. Karmakar, "Smart sensing: Chipless RFID solutions for the Internet of Everything," *IEEE Microwave Magazine*, vol. 16, no. 10, pp. 26–39, 2015.
14. A. Marindra, G. T.-I. T. on Microwave, and undefined 2018, "Chipless RFID sensor tag for metal crack detection and characterization," *ieeexplore.ieee.orgAMJ Marindra, GY TianIEEE Transactions on Microwave Theory and Techniques, 2018•ieeexplore.ieee.org*, Accessed: Dec. 06, 2023. [Online].Available:https://sci-hub.ren/https://ieeexplore.ieee.org/abstract/ document/8307772/

15. K. Brinker and R. Zoughi, “Tunable chipless RFID pressure sensor utilizing additive manufacturing,” in *2022 IEEE International Instrumentation and Measurement Technology Conference (I2MTC)*, 2022, pp. 1–6.
16. B. A. Farhan, “Design and Implementation of an Automatic Transfer Switch for a Single Phase Power Generator,” no. 7, pp. 16–20, 2021.